Available online at www.sciencedirect.com
SCIENCE DIRECT®
Journal of the European Ceramic Society 26 (2006) 1–7
www.elsevier.com/locate/jeurceramsoc

Silver nanoparticles supported on α-, η- and δ-alumina

A. Esteban-Cubillo[a], C. Díaz[b], A. Fernández[b], L.A. Díaz[b], C. Pecharromán[a], R. Torrecillas[b], J.S. Moya[a,*]

[a] *Instituto de Ciencia de Materiales de Madrid (ICMM)-CSIC, Cantoblanco, 28049 Madrid, Spain*
[b] *Instituto Nacional del Carbón (INCAR)-CSIC, Francisco Pintado Fe 26-33011 Oviedo, Spain*

Received 18 July 2004; received in revised form 12 October 2004; accepted 24 October 2004
Available online 5 January 2005

Abstract

Silver monodispersed nanopaticles supported on α- and η-Al_2O_3 have been obtained by a colloidal processing route. Precursor (silver acetate) was transformed into Ag metallic nanoparticles deposited on Al_2O_3 powder after a drying and reduction process. Silver particle size varies between 100 and 1 nm depending on the alumina phase. On the basis of HRTEM studies, and according to the nature of alumina surface, a mechanism of nucleation and growth of silver nanoparticles has been proposed. Finally, optical spectra of these samples revealed the presence of silver surface plasmon, which supplies information about the dispersion of nanoparticles into alumina matrices.

Keywords: Al_2O_3; Nanocomposites; Optical properties; Ag

1. Introduction

Nanoscience and nanotechnology are two disciplines, evolving at present from an experimental state to industrial production. However, up to now, the preparation of large quantities of heterogeneous materials containing monodisperse nanoparticles is becoming one of the bottlenecks that hinders the development of commercial devices. In that sense, many references can be found in the literature describing nanoparticles preparation methods which only remain monodispersed and non-aglomerated in liquid suspensions[1–4] (colloids) or embedded in rigid matrices.[5,6] Moreover, it is quite common, that nanoparticles, due to their large surface energy, induce aggregation processes, specially when they appear as a powdered single-phase, for example, after drying a colloidal suspension. In the case that the individual character of the nanoparticles is a crucial characteristic for the application (optical applications), colloidal methods cannot be employed straightforwardly. In fact, nanoparticles must be isolated, coated[1] or "frozen" in a matrix, before being characterized or measured.

A similar mechanism has been used since historical times to produce coloured glasses by dispersing very small metallic particles into a melted glass and quenching it afterwards.[7] The presence of the colour is a consequence of surface plasmon resonances in these nanoparticles. These excitations can be described as charge oscillations due to a large enhancement of the local electric field inside the metallic particles. This large local electric field is also responsible for the anomalous large non-linear component of the optical refractive index of composites of Au, Cu or Ag nanoparticles embedded into a ceramic matrix. In that sense, a large increase of χ,[3] the non-linear dielectric susceptibility,[8] has been reported for composites prepared by several epitaxial preparation procedures.

Additionally, surface plasmons present in insulator–metal nanostructured materials are responsible for the so-called surface-enhanced Raman spectroscopy (SERS)[9,10] and surface-enhanced infrared absorption (SEIRA)[11] and offer the possibility to be applied in microelectronics[12] and storage of optic data.

* Corresponding author. Tel.: +34 913349000; fax: +34 913720623.
E-mail address: jsmoya@icmm.csic.es (J.S. Moya).

0955-2219/$ – see front matter © 2004 Elsevier Ltd. All rights reserved.
doi:10.1016/j.jeurceramsoc.2004.10.029

In this work, we have investigate the possibility to prepare a large quantity of metallic nanoparticles supported on dielectric matrices in order to be able to handle them avoiding agglomeration processes and possible health problems. Recently, Oberdörster et al.[13] have reported the possible harmful character of nanoparticles <100 nm in size. One of the advantages of the proposed route is that the nanoparticles are attached to micron-sized or submicron-sized inert (ceramic) particles. Once the powder bearing nanoparticles is prepared, it may be dispersed into transparent matrices (taking into account that their refractive index must be similar to that of the powder particles) to be used for optical applications. In this paper, we have focused the influence of the alumina phase on size, morphology and dispersion of the silver nanoparticles. It should be noted, that the alumina/silver system has been widely studied for catalytic applications, specifically in the reaction of epoxidation of ethylene through silver-catalyzed[14,15] and the hydrogenation of aromatic compounds.[16,17] However, to our knowledge, there is no systematic description in the literature about the nanoparticle morphology, which is a crucial issue in order to employ this kind of material in emerging technologies.

2. Experimental procedure

Silver metallic nanoparticles supported on alumina were obtained by a colloidal processing route, starting from silver acetate (Aldrich) and different alumina submicron-size powders: α-Al_2O_3 (AA04 Sumitomo, Japan), η-Al_2O_3 (Sumitomo, Japan) obtained by dehydroxilation of the oxhydroxide precursor (bayerite)[18] and δ-Al_2O_3 (Teclink, Germany) produced by a high-temperature plasma spraying as precursors.

The Brunauer–Emmet–Teller (BET) specific surface area of the different aluminas was determined using FlowSorb II 2300 equipment.

The nanoparticles were deposited on alumina powders by mixing a silver acetate solution (3 M) with a suspension of alumina powder, so that the final relative silver concentration on alumina was 1 vol.%. The resulting suspension was heated at 70 °C with constant magnetic agitation to homogenize it, and subsequently dried at 120 °C in a stove for 24 h to eliminate the solvent. As a result, silver oxide (I) nanoparticles deposited on alumina particles were obtained. Once dry, the powder was reduced in a 90%Ar/10%H_2 atmosphere at 350 °C for 2 h to obtain finally coloured powders.

The resulting powders were analyzed by X-ray diffraction (Bruker AXS Mod. D8 Advance with Cu Kα radiation). The silver particle size and the morphological aspects of the different powders were studied by transmission electron microscopy using a JEOL FXII, JEM 2000 both operating at 200 keV and a JEOL ARM HRTEM operating up to 1250 keV.

Finally, the surface plasmon of the silver nanoparticles was determined by measuring the diffuse reflectance of pure KBr pressed pellets painted with an acetone α-, η-, δ-alumina/nAg suspension in a Cary 500 Spectrometer fitted with a diffuse reflectance cell. Conversion from diffuse reflectance to absorbance units were done by the well know Kulbeka–Munk expression.[19]

3. Results

The X-ray diffraction patterns corresponding to the alumina/nAg are shown in Fig. 1. As can be observed, metallic silver Bragg reflexions appear on the three diffractograms considered. It is worth mentioning that the broader Ag diffraction peak is the one corresponding to η-Al_2O_3/nAg (Fig. 1B). This fact indicates that in this particular sample the silver nanoparticles have the smallest average crystallite size.

The optical spectra of the samples were measured by diffuse reflectance from 300 to 750 nm (Fig. 2). It is well known that silver nanoparticles display a surface plasmon around 400 nm. However, the precise position and shape of the band depends on the environment of the nanoparticles. The α-Al_2O_3/nAg sample shows a maximum and a shoulder at 404 and 368 nm, respectively. In the case of η-Al_2O_3/nAg, the maximum is much wider. Finally, the δ-Al_2O_3/nAg sample presents a maximum centered at 400 nm but no evidence of the shoulder was found.

The morphology of the samples was studied by HRTEM. As can be observed in Fig. 3, silver nanocrystals (10–20 nm diameter) sit on the surface of the α-Al_2O_3 particles. A close view of the silver alumina interface reveals a thin amorphous phase (∼4 nm thickness) completely covering the alumina particle surface, which is in contact with silver (Fig. 4). In fact this layer covers the totality of the α-Al_2O_3 particles.

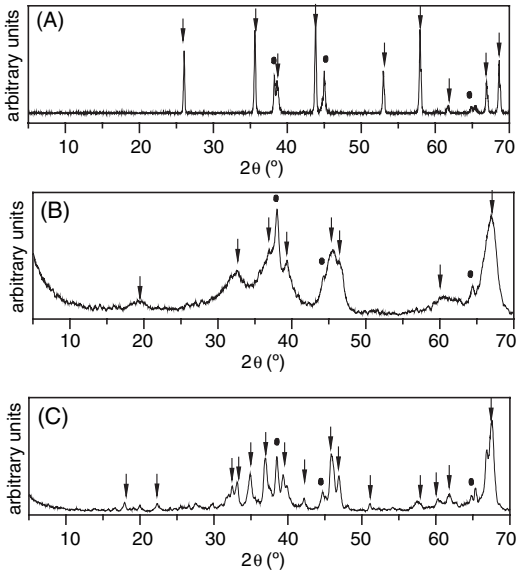

Fig. 1. XRD powder patterns corresponding to: (A) α-Al_2O_3/nAg, (B) η-Al_2O_3/nAg and (C) δ-Al_2O_3/nAg. Alumina and silver diffraction peaks have been indicated by vertical arrows and dots, respectively.

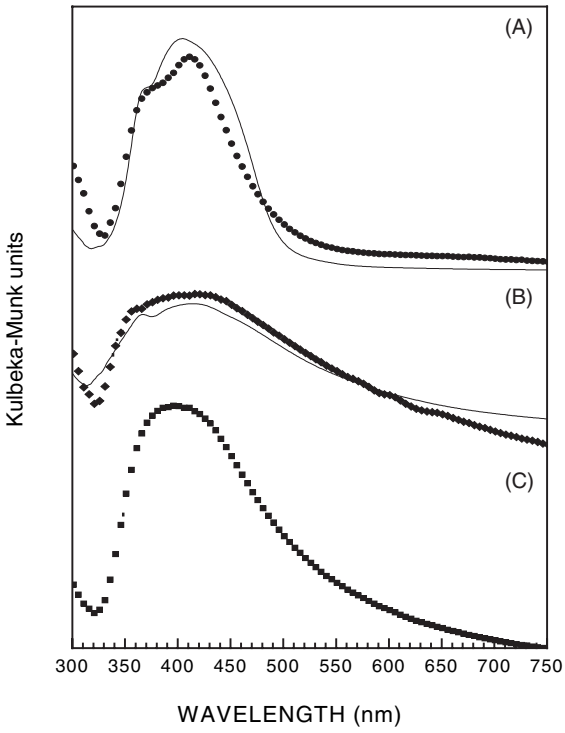

Fig. 2. Experimental (dots) and fitted (continuous lines) absorption spectra taken by diffuse reflectance measurements of silver nanoparticles dispersed on: (A) α-Al_2O_3, (B) η-Al_2O_3 and (C) δ-Al_2O_3.

The η-Al_2O_3 is the least crystalline and the most porous phase of the three phases considered as can be observed in the X-ray diffractogram (Fig. 1) and by TEM analysis (Fig. 5). Its specific BET surface area was found to be 151 m^2/g, i.e. about two orders of magnitude higher than that of α-Al_2O_3 (3 m^2/g) and much higher than that of δ-Al_2O_3 (36 m^2/g). In this sample, the silver nanocrystals are difficult to detect due to their small size. Only a few silver single crystals was found after several session of HRTEM (Fig. 6).

In the case of δ-Al_2O_3/nAg powder, a large fraction of silver particles have sizes larger than 20 nm, which correspond to those, which nucleate and grow outside the alumina particle surfaces. The smaller silver nanoparticles are located only

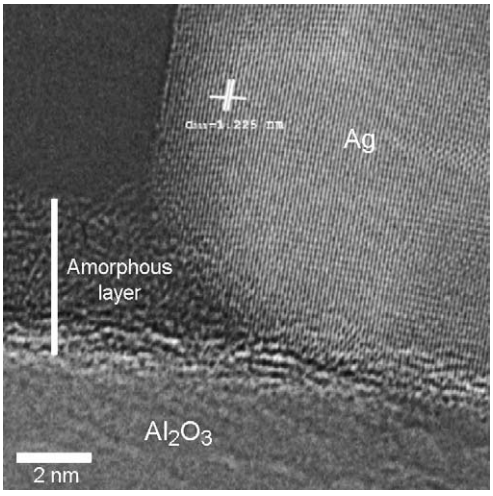

Fig. 4. HRTEM micrograph of α-Al_2O_3/nAg interphase at two different magnifications.

in specific regions of the δ-Al_2O_3 surfaces, corresponding to rough regions as seen in Fig. 7A and B. It is also worth mentioning the complete absence of an amorphous coating on the spherical δ-Al_2O_3 particles (Fig. 8).

4. Discussion

The mechanism operating at the silver nanoparticles deposit can be described as follows: the silver acetate appears totally dissociated,[20] so that silver cations are able to be chemisorbed through OH^- sites on the alumina surface.[18,21] During the drying stage, the chemisorbed cations could play the role of nucleation centres driving the silver growth process.

In the case of the δ-phase, the alumina particles seem to be free of any hydrated coating (Fig. 8). On the other hand, as observed in Fig. 7A and B, only few silver nanoparticles were found attached to δ-Al_2O_3 particles, mainly at surface regions with facetted interfaces. It is expected[18] that those places have the highest surface energy so that it is likely

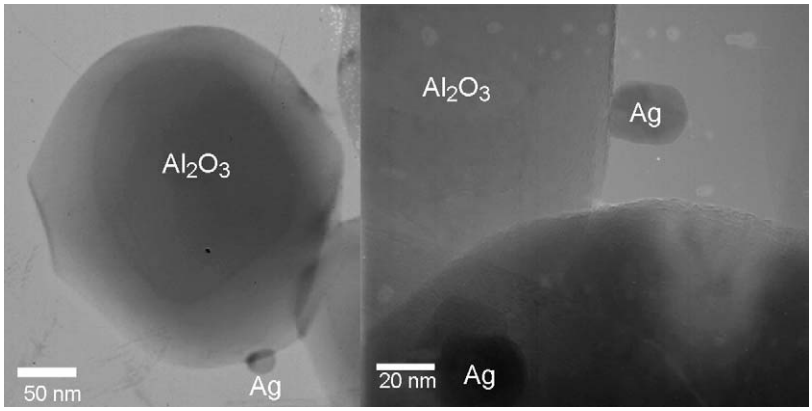

Fig. 3. TEM micrographs corresponding to silver nanoparticle on the surface of α-Al_2O_3 at two different magnifications.

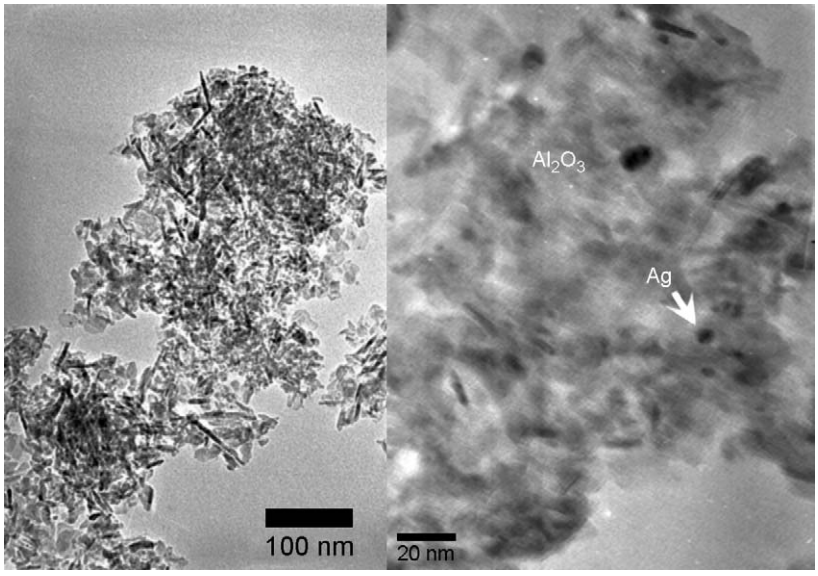

Fig. 5. TEM micrographs of η-Al_2O_3/nAg.

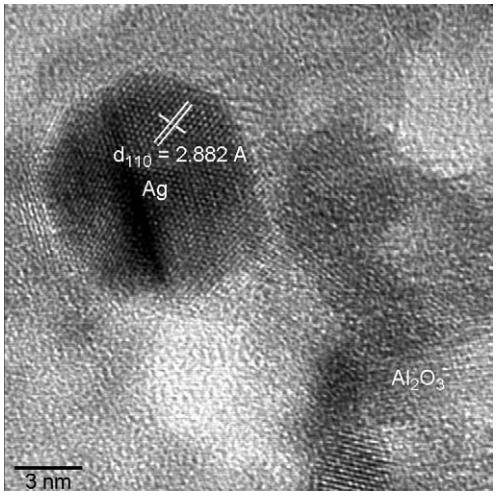

Fig. 6. HRTEM micrograph of η-Al_2O_3/nAg.

that silver cations would precipitate there to stabilize those regions. However, the availability of such nucleation centres on δ-Al_2O_3 is limited so that a large proportion of coarse silver particles must grow outside of the δ-alumina surface (Fig. 7A).

As a consequence of the synthesis process, η-Al_2O_3 particles appear as poorly crystallized aggregates, with a large fraction of open porosity (BET = 151 m^2/g). In this sense, we think that silver cations can interact over the large area of highly active alumina to produce a large number of very small Ag_2O nucleation centres. In fact, this phase presents the smallest particle size, <5 nm (Fig. 5), of the three Ag/Al_2O_3 samples considered. Moreover, according to the contrast and texture of Ag nanoparticles, we believe that most of them lie inside the pores of the η-Al_2O_3 particles.

Finally the α-phase is an intermediate case between η and δ. The crystallites are relatively large (approximately

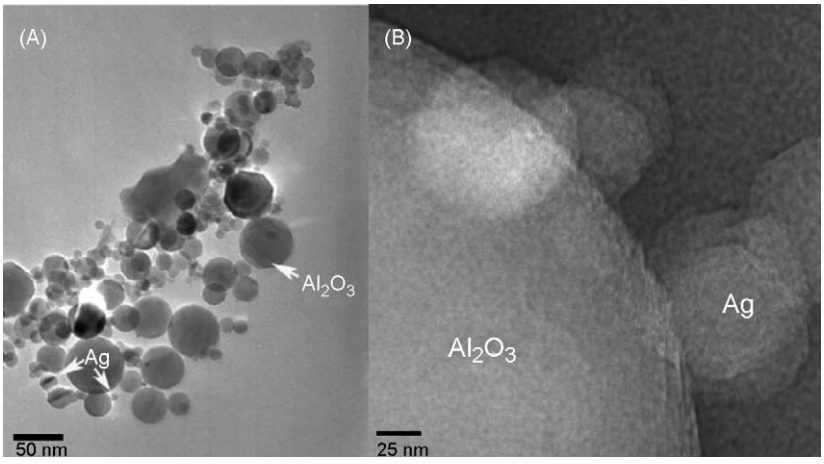

Fig. 7. TEM micrographs of δ-Al_2O_3/nAg (A) and silver nanoparticles attached on a facetted interface of δ-Al_2O_3 (B).

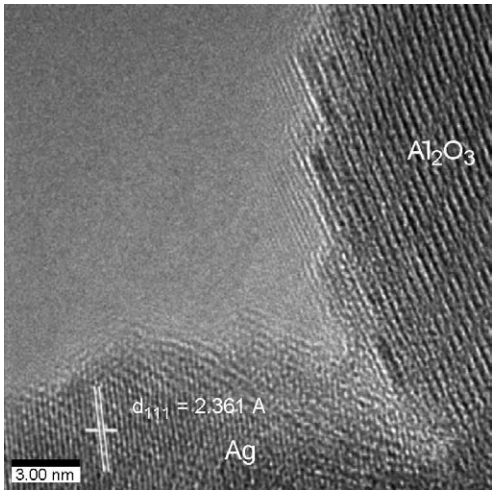

Fig. 8. HRTEM micrograph of δ-Al_2O_3/nAg.

300 nm) but its surface appears to be coated by a hydroxide layer (Fig. 4) as a consequence of the processing of powder in distilled water, as has previously been pointed out.[18] In that sense, we think that the silver precursor tends to precipitate over this hydroxide layer following a similar mechanism as in the η-phase.

α-Al_2O_3/nAg displays a greenish tonality corresponding to the sharp plasmon effect of silver at 410 nm (Fig. 2). The dark brown colour of η-Al_2O_3/nAg is a consequence of the large maximum observed in Fig. 2, while the δ-Al_2O_3/nAg displays a green-brown colour, in agreement with its large plasmon half-width maximum. Diffuse reflectance spectra of Al_2O_3/nAg (named as R) were used to get quantitative information about the surface plasmon absorption maximum and to correlate it with information about size, homogeneity and local environment of the silver nanoparticles. For the sake of convenience, the reflectance spectra were transformed according to the Kulbeka–Munk relationship for absorbance ($A = 2R/(1-R)$). In Fig. 2 the spectra of the three alumina phases with silver nanoparticles are shown. All of them present strong absorbance maxima corresponding to silver surface plasmons. In a system of highly diluted spherical nanoparticles, the surface plasmon condition is verified when the real part of the dielectric constant of the metal satisfies,

$$\varepsilon_{Ag}(\lambda) = -2\varepsilon_m \tag{1}$$

where ε_{Ag} and ε_m are the dielectric constant of silver and of the matrix, respectively. Thus, for dilute systems, the absorption maximum depends on ε_m. A more precise evaluation of the plasmon absorption, using the quasistatic approximation $r \ll \lambda$ (where r and λ are the nanoparticle radius and the wavelength, respectively) and an effective medium approximation[22] to calculate the dielectric constant of the metal/insulator composite, shows that for increasing metal concentration, the position of the peak shifts to longer wavelengths while the whole peak broadens.[23] The effective medium used, which is a generalization of the well known

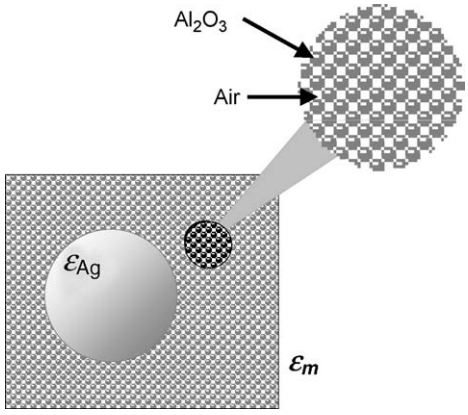

Fig. 9. Scheme of the three-phase model: silver–alumina–air. Silver particles are embedded into a composite matrix made of alumina and air.

Bruggeman model[24] can be written as:

$$(1-f)\left(\frac{2(\langle\varepsilon\rangle-\varepsilon_m)}{(1-L_m)\langle\varepsilon\rangle+L_m\varepsilon_m}+\frac{(\langle\varepsilon\rangle-\varepsilon_m)}{2L_m\langle\varepsilon\rangle+(1-2L_m)\varepsilon_m}\right) + 9f\frac{\langle\varepsilon\rangle-\varepsilon_{Ag}}{2\langle\varepsilon\rangle+\varepsilon_{Ag}} = 0 \tag{2}$$

where $\langle\varepsilon\rangle$ is the effective dielectric constant; f, silver volume concentration; ε_{Ag} and ε_m, dielectric constant and L_m, depolarization factor of the matrix particles which becomes $L_m = 1/3$ in the case of spherical particles. This latter condition corresponds to the original Bruggemann approximation.[24] In this paper we have disregarded the possibility to have a large amount of non-spherical silver nanoparticles due to the fact that the plasmon curves present a single maximum and HRTEM does not detects the presence of oblate or prolate particles (which present two surfaces plasmon resonance).[4]

However, special care has been taken to properly evaluate the effective value of the matrix dielectric constant. Thus, a three-phase system (air–alumina–silver) (Fig. 9) must be considered to accurately reproduce the optical spectra of the corresponding samples. For a sake of simplicity we have determined the effective dielectric constant of the matrix by the Bruggeeman approximation, which is very similar to that used to calculate the optical spectrum.

$$(1-\phi)\frac{\varepsilon_m-\varepsilon_{alum}}{2\varepsilon_m+\varepsilon_{alum}}+\phi\frac{\varepsilon_m-1}{2\varepsilon_m+1}=0 \tag{3}$$

being $\varepsilon_m = 1$ and $\varepsilon_{alum} = 3.3$ the dielectric constant of air and alumina, respectively, and ϕ the local alumina concentration around the silver surface. The simultaneous fit of Eqs. (2) and (3) to experimental spectrum will allow both the effective concentration of silver particles, f, and the porosity of the matrix $(1-\phi)$ to be determined due to the fact that according to Eq. (1), the position of the absorption maximum of the surface plasmon corresponding to embedded metallic spheres depends on the dielectric constant of the matrix, ε_m. This effective matrix dielectric constant is then related to the

local environment of the nanoparticles. In fact, the dielectric constant of the matrix would be that of alumina at optical frequencies ($\varepsilon_m \sim 3.3$)[25] only in case of silver particles embedded into dense alumina matrices ($\phi = 1$). However, this is not so, because, in the case of the η-phase of alumina, some degree of porosity is seen. Moreover, for the dense alumina particles (α and δ), the silver nanoparticles precipitate on the alumina surface, in such a way that one half of the silver surface has an alumina/silver interface, while the rest of the nanoparticle is limited by an air/silver interface. This situation would correspond to a value of $\phi = 0.5$.

In order to evaluate the effective medium approximation, optical constant of alumina[25] and silver[26,27] obtained from the literature have been used.

In the case of the α-Al_2O_3 matrix particles, a dielectric constant of $\varepsilon_m = 1.85$ successfully reproduce the experimental spectra, which approximately corresponds to a mixture of 50/50 vol.% of air and alumina according to Eq. (3). The silver filling factor obtained by fitting was $f = 0.025$. Those parameters suggest that all silver nanoparticles precipitated only on the corundum grain surfaces, so that every single particle has the same environment, i.e. air along the exterior region of the particle and alumina in the interior. The fitted filling factor is 2.5 times larger than that of the nominal value. However, a similar effect has been previously found in mixtures with large differences in the particle size. In fact it has been postulated that if small particles, which have a mean radius of r, appears on the surface of the large particles, having a radius of R, the available volume for them reduces to a spherical shell of thickness r around the spherical surface of radius R.[28] It can be stated that the local filling factor is increased by a factor of $R/(3r)$. Taking into account that the ratio between the α-Al_2O_3 and the Ag particles (Fig. 3) is $R/r = 10$, then a local concentration of $f_{local} = f \cdot 10/3 = 0.03$ may be expected, in good agreement with the value $f = 0.025$ obtained from fitting to optical measurements.

The peak of the surface plasmon of η-Al_2O_3 is the broadest one. This broadening may be due to: (i) the large value of the local volume concentration or (ii) to a modification of the dielectric constant of silver due to the small particle size.[29] We had to disregard the first hypothesis because no successful fit was obtained using the dielectric constant of bulk silver. Instead, we should use the dielectric constant deduced by Kreibig's modification[29] of the Drude theory, in order to reproduce the experimental spectrum.

$$\varepsilon(\omega) = \varepsilon_\infty + \varepsilon_{ie}(\omega) - \frac{\omega_P^2}{\omega^2 + i\omega(\gamma_0 + v_F/r)} \quad (4)$$

where $\omega = 2\pi c/\lambda$, $\varepsilon_\infty = 4$, $\omega_P = 1.4 \times 10^{16}\ s^{-1}$, is the plasma frequency of silver, $\gamma_0 = 1/\tau_s = 2.94 \times 10^{13}\ s^{-1}$ is the reciprocal of the collision time, and $v_F = 1.4 \times 10^6\ m\ s^{-1}$ is the Fermi velocity.[30] Expression (4) takes into account the modification of the mean free path of the electrons due to collisions with the particle surface. However, this free electron model does not take into account the high frequency features of the refractive index due to the internal levels electronic transition. We have labelled this term as $\varepsilon_{ie}(\omega)$ and it is expected to show no appreciably change with particle size for particles large than 1 nm. The term $\varepsilon_{ie}(\omega)$ can be easily estimated as:

$$\varepsilon_{ie}(\omega) = \varepsilon_{exp}(\omega) - \varepsilon_\infty + \frac{\omega_P^2}{\omega^2 + i\omega\gamma_0} \quad (5)$$

where $\varepsilon_{exp}(\omega)$ corresponds to the experimentally determined dielectric constant for bulk silver.[26] Introducing Eq. (5) into (4) it can be written as:

$$\varepsilon(\omega) = \varepsilon_{exp}(\omega) - \omega_P^2 \left[\frac{1}{\omega^2 + i\omega(\gamma_0 + v_F/r)} - \frac{1}{\omega^2 + i\omega\gamma_0} \right] \quad (6)$$

According to a numerical evaluation of expression (6), only particles smaller that 7 nm will display appreciable variations of the dielectric constant for silver. In this sense, we have found that the best fit was attained when the particle diameter was $2r = 1.3$ nm, the silver concentration $f = 0.01$ and the external dielectric constant $\varepsilon_m = 2.3$ which approximately corresponds to a surrounding medium composed of alumina/air with a porosity of 30%. These parameters agree reasonably well with TEM observations, that is, silver particles are embedded in porous η-Al_2O_3 particles. It should be noted that according to the particle size obtained by the fit of the optical spectra of silver deposited on η-Al_2O_3, the degree of electronic confinement in these silver nanoparticles must be very high. In fact, large enhancements of the non-linear susceptibility in this sample[31] could be expected especially at the region of the spectrum around the surface plasmon resonance.

The spectrum of silver nanoparticles on δ-Al_2O_3 powder was not fitted to the expression (2) because of the wide size distribution observed by TEM, which prevents us from using the low wavelength approximation. In fact, the absence of the 370 nm shoulder, present in the α- and η-Al_2O_3 samples, may be related to Mie scattering from some of the large free silver particles, which can blur the spectrum.

5. Conclusions

Silver monodispersed nanoparticles supported on α- and η-Al_2O_3 have been obtained by a simple low cost colloidal route. Silver nanoparticle size <5 nm for η-alumina, 10–20 nm for α-alumina and >20 nm for δ-alumina phase were obtained. On the basis of HRTEM studies, a mechanism of nucleation and growth of the silver nanoparticles according to the nature of the alumina surface have been proposed. Finally, optical spectra on these samples revealed the presence of a silver nanoparticle surface plasmon, which supplies information about the dispersion of the silver nanoparticles on the different alumina powders.

Acknowledgements

This work has been supported by the Spanish Ministry of Science and Technology under Project No. MAT2003-04199-C02-01. We thanks to Dr. Gunther Richter at Institute für Metallforschung of Max Planck Institute at Stuttgart (Germany) and Dr. L. Gremillard (LBNL, Berkeley, CA, USA) for assistance in HRTEM.

References

1. Ung, T., Liz-Marzán, L. M. and Mulvaney, P., Optical properties of thin films of Au@SiO_2 particles. *J. Phys. Chem. B*, 2001, **105**, 3441–3452.
2. García-Vidal, F. J., Pitarke, J. M. and Pendry, J. B., Silver-filled carbon nanotubes used as spectroscopic enhacers. *Phys. Rev. B*, 1998, **58**(11), 6783–6786.
3. Lalande, J., Scheppokat, S., Janssen, R. and Claussen, N., Toughening of alumina/zirconia ceramic composites with silver particles. *J. Eur. Ceram. Soc.*, 2002, **22**, 2165–2171.
4. Link, S. and El-Sayed, M. A., Spectral properties and relaxation dynamics of surface plasmon electric oscillations in gold and silver nanodots and nanorods. *J. Phys. Chem. B*, 1999, **103**, 8410–8426.
5. Barnes, J.-P., Petford-Long, A. k., Doole, R. C., Serna, R., Gonzalo, J., Suárez-García, A. *et al.*, Structural studies of Ag nanocrystals embedded in amorphous Al_2O_3 grown by pulsed laser deposition. *Nanotechnology*, 2002, **13**, 465–470.
6. Naser, J. and Ferkel, H., Laser-induced synthesis of Al_2O_3/Cu-nanoparticule mixtures. *NanoStruct. Mater.*, 1999, **12**, 451–454.
7. Pérez-Arantegui, J., Molera, J., Larrea, A., Pradell, T., Vendrell-Sanz, M., Borgia, I. *et al.*, Luster pottery from the thirteenth century to the sixteenth century: a nanostructured thin metallic film. *J. Am. Ceram. Soc.*, 2001, **84**(2), 442–446.
8. Ung, T., Liz-Marzán, L. M. and Mulvaney, P., Gold nanoparticle thin films. *Colloids Surf. A*, 2002, **202**, 119–126.
9. Chumanov, G., Sokolov, K., Gregory, B. W. and Cotton, T. M., Colloidal metal films as a substrate for surface-enhaced spectroscopy. *J. Phys. Chem.*, 1995, **99**, 9466–9471.
10. Freeman, G. R., Grabar, K. C., Allison, K. J., Bright, R. M., Davis, J. A., Guthrie, A. P. *et al.*, Self-assembled metal colloid monolayers—an approach to sers substrates. *Science*, 1995, **267**, 1629–1632.
11. Pecharromán, C., Cuesta, A. and Gutiérrez, C., Calculation of adsorption-induced differential external reflectance infrared spectra of particulate metals deposited on a substrate. *J. Electroanal. Chem.*, 2004, **563**, 91–109.
12. Kepley, L. J., Sackett, D. D., Bell, C. M. and Mallouk, T. E., Metal–insulator–semiconductor and metal–insulator–metal devices derived from zirconium phosphonate thin films. *Thin Solid Films*, 1992, **208**, 132.
13. Oberdörster, G. *et al.*, Headache for nanoparticles. *Mater. Today*, 2004, 10.
14. Miyadera, T., Selective reduction of nitric oxide with ethanol over an alumina-supported silver catayst. *Appl. Catal. B*, 1997, **13**, 157–165.
15. Ayame, A., Uchida, Y., Ono, H., Miyamoto, M., Sato, T. and Hayasaka, H., Epoxidation of ethylene over silver catalysts supported on alfa-alumina crystal carries. *Appl. Catal. A: Gen.*, 2003, **244**, 59–70.
16. Boudjahem, A.-G., Monteverdi, S., Mercy, M., Ghanbaja, D. and Bettahar, M. M., Nickel nanoparticles supported on silica of low surface area. Hydrogen chemisorption and TPD and catalytic properties. *Catal. Lett.*, 2002, **84**, 115–121.
17. Molina, R. and Poncelet, G., Hydrogenation of benzene over alumina-supported nickel catalysts prepared from Ni(II) acetylacetonate. *J. Catal.*, 2001, **199**, 162–170.
18. Wefers, K. and Misra, C., *Oxides and Hydroxides of Alumium. Alcoa Technical Paper 19; Revised*. Alcoa Laboratories, Pittsburgh, PA, 1987.
19. Kortüm, G., *Reflectance Spectroscopy*, transl. J. E. Lohr. Spinger-Verlag, Berlin, 1969, pp. 103–163, chapter IV.
20. Lide, D. R., In *Handbook of Chemistry and Physics (82nd ed.)*, ed. E. D. Chief. CRC Press, Boca Raton, FL, 2002, pp. 8–123.
21. Kotomin, E. A., Maier, J., Zhukovskii, Y. F., Fuks, D. and Dorfman, S., Ab initio modelling of silver adhesion on the corundum (0 0 0 1) surface. *Mater. Sci. Eng. C*, 2003, **23**, 247–252.
22. Pecharromán, C. and Iglesias, J. E., Effective dielectric properties of packed mixtures of insulator particles. *Phys. Rev. B*, 1994, **49**, 7137.
23. Gordillo, F. and Pecharromán, C., Optical properties of binary composite materials with two nonlinear components. *J. Modern Opt.*, 2003, **50**, 1857.
24. Bruggeman, D. A. G., *Ann. Phys. (Leipzig)*, 1935, **24**, 636.
25. Gervais, F., *Handbook of Optical Properties of Solids, Vol 2*, ed. E. D. Palik. Academic Press, San Diego, 1991, p. 761.
26. Lynch, D. W. and Hunter, W. R., In *Handbook of Optical Constants of Solids*, ed. E. D. Palik. Academic Press, Orlando, 1985, p. 350.
27. Johnson, P. B. and Christy, R. W., Optical constanta of the noble metals. *Phys. Rev. B*, 1972, **6**, 4370.
28. Pecharromán, C. and Iglesias, J. E., Modeling particle size and clumping effects in the IR adsorbance spectra of dilute powders. *Appl. Spectrosc.*, 1996, **50**, 1553–1562.
29. Kreibig, U. and Fragstein, C. V., The limitation of electron mean free path in small silver particles. *Z. Phys.*, 1969, **224**, 308.
30. Reynolds, F. W. and Stilwell, G. R., Mean free paths of electrons in evaporated metal films. *Phys. Rev.*, 1952, **88**, 418.
31. Flytzanis, C., Hache, F., Kelin, M. C., Ricard, D. and y Roussignol, P., Nonlinear optics in composite-materials. 1. Semiconductor and metal crystallites in dielectrics. *Prog. Optics*, 1991, **29**, 322.